INORGANIC CHEMISTRY FRONTIERS

RESEARCH ARTICLE

View Article Online
View Journal | View Issue

Check for updates

Cite this: *Inorg. Chem. Front.*, 2023, **10**, 3940

# Synthesis, kinetic studies, and atom transfer reactivity of [2Fe–2E] model compounds†

Erwin A. Weerawardhana,[a] Matthias Zeller[b] and Wei-Tsung Lee *[a]

Received 24th April 2023,
Accepted 1st June 2023

DOI: 10.1039/d3qi00728f

rsc.li/frontiers-inorganic

The synthesis of [2Fe–2E] (E = S and Se) complexes supported by an *N*-alkyl,*N*′-aryl-β-diketiminate ligand is described. The [2Fe–2S] model compound has an unusually long Fe···Fe distance, but the equivalent distance in the [2Fe–2Se] compound is comparable to those reported in the literature. These model compounds display varying electron transfer capabilities, which were elucidated through electronic spectroscopy and electrochemical analysis. Kinetic data and activation parameters suggest the formation mechanism of the [2Fe–2S] compound. Additionally, to probe the possible sulfur-transfer mechanism of [2Fe–2S] clusters, atom transfer reactivity was pursued.

Published on 01 ervna 2023. Downloaded on 01.02.2026 21:36:21.

## Introduction

Iron–sulfur clusters ([*m*Fe–*n*S], where *m* and *n* = 2–4) form redox active, multiple-metal cofactors in the active sites of many enzymes. These clusters are often viewed as special inorganic cofactors and elicit a variety of biological functions, including electron transfer, sensing, and regulation.[1–4] A majority of the functions of such clusters stem from their redox reactivity. The electronic structure of iron–sulfur clusters has been widely studied and it was found that the oxidation state of iron centers commonly ranges from +2 to +3,[1,5] which contrasts with the higher oxidation states found in heme systems. A common structural feature of these clusters is that each iron center is coordinated by four donor atoms (N-donor or S-donor) in a tetrahedral environment.[1]

Although many functions of iron–sulfur clusters are considered well-understood, there are two newly emerging interests in this area: (1) the exploration of new biological functions of iron–sulfur clusters, and (2) understanding the electronic origins of the chemistry of iron–sulfur *versus* iron–selenium clusters and how these may influence or determine enzyme function and mechanism. For example, the sulfur-atom transfer involving an iron–sulfur cluster in the last step of the biotin biosynthetic pathway has long been debated.[6–11] In addition, several studies have shown that sulfur atoms can be substituted by selenium in iron–sulfur clusters while retaining structural integrity.[12–14] Studying iron–selenium clusters or related model compounds could yield valuable information as to why S has been universally selected to function in these clusters over Se at the active sites of enzymes.[15,16]

Researchers have extensively explored structure–function relationships of naturally occurring iron–sulfur clusters. Synthetic model iron sulfur compounds can provide additional insight into the complexity of the natural systems. While continuous efforts have led to the successful synthesis of [3Fe–4S] and [4Fe–4S] model clusters,[17,18] methods to make and study [2Fe–2E] (where E = S and Se) models are less developed.[11–14] The production of synthetic [2Fe–2S/Se] clusters with supporting chalcogenide ligand and its effect on spectroscopy and reduction potentials of natural systems has been reported.[9] Due to the coordination arrangement, some bidentate ligands have been successfully demonstrated to mimic the [2Fe–2S] active site of enzymes.[19–24] More recently, bidentate β-diketiminates were used to synthesize [2Fe–2S] clusters owing to their high tunability as supporting ligands.[25–27] [2Fe–2Se] model systems supported by the nitrogen donor ligands are however rather rare (Scheme 1).[23,28,29]

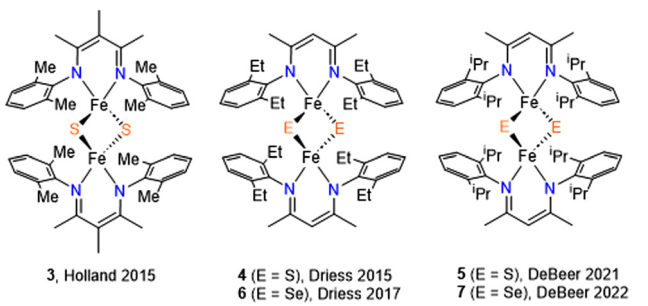


**Scheme 1** [2Fe–2S] and [2Fe–2Se] model compounds supported by β-diketiminate ligands.

[a]*Department of Chemistry and Biochemistry, Loyola University Chicago, Chicago, Illinois 60660, USA. E-mail: wlee5@luc.edu*
[b]*Department of Chemistry, Purdue University, West Lafayette, IN 47907, USA*

†Electronic supplementary information (ESI) available. CCDC 2252043 and 2252044. For ESI and crystallographic data in CIF or other electronic format see DOI: https://doi.org/10.1039/d3qi00728f


This journal is © the Partner Organisations 2023

Published on 01 ervna 2023. Downloaded on 01.02.2026 21:36:21.

We recently reported an asymmetric *N*-alkyl,*N*′-aryl-β-diketiminate (**L1**) ligand and its low-valent iron complex[30] as a suitable candidate for preparing [2Fe–2E] model compounds. Herein we report the synthesis of [2Fe–2E] model compounds **1** and **2**, which were characterized by X-ray crystallography, $^1$H-NMR spectroscopy, and electrochemical studies. In the context of the recent advances in [2Fe–2E] model compounds, our objective was to gain a deeper understanding of their formation from low-valent iron precursors and elemental sulfur. Thus, we conducted kinetic experiments to investigate the kinetic isotopic effect and activation parameters involved in the reaction of an Fe(I) complex with elemental sulfur, resulting in the formation of **1**. Moreover, in light of the unusually long Fe···Fe distance noted in **1**, further investigations were performed to explore the atom transfer reactions.

# Experimental section

### Materials and methods

All manipulations were performed under a nitrogen atmosphere using standard Schlenk techniques or in an M. Braun UNIlab Pro glovebox. Glassware was dried at 150 °C overnight. Diethyl ether, *n*-pentane, tetrahydrofuran, and toluene were purified using a pure process technology solvent purification system. Before use, an aliquot of each solvent was tested with a drop of sodium benzophenone ketyl in THF solution. All reagents were purchased from commercial vendors and used as received. (**L1**)Fe(cod) (cod = 1,5-cyclooctadiene) was prepared according to a literature procedure.[30] $^1$H NMR data were recorded on a Varian Inova 500 MHz spectrometer at 22 °C. Resonances in the $^1$H NMR spectra are referenced to residual $C_6D_5H$ at $\delta$ = 7.16 ppm. Solution magnetic susceptibilities were determined using the Evans method.[31] UV-vis spectra were recorded on an Agilent Cary 8454 UV-vis spectrophotometer equipped with a Unisoku Scientific Instruments Cryostat USP-203B for various temperature experiments. An IR spectrum of **1** was recorded on a Jasco FT-IR spectrometer (model 4600) equipped with an ATR diamond probe head. Elemental analysis was conducted by Midwest Microlab, LLC (Indianapolis, IN).

### Synthetic procedures

**[(L1)Fe(μ-S)]$_2$ (1).** To a stirred solution of $S_8$ (49 mg, 0.19 mmol) in toluene (5 mL) at ambient temperature under $N_2$ atmosphere was added a solution of LFe$^I$(cod) (100 mg, 0.19 mmol) in toluene (10 mL) for 24 h. The reaction mixture was filtered twice through $Al_2O_3$. Volatiles were removed under reduced pressure, and the residue was extracted with *n*-pentane and filtered through Celite. The filtrate was dried *in vacuo* to yield a dark purple solid (42 mg, 49%). Crystals suitable for X-ray diffraction were grown from a concentrated solution in *n*-pentane at −20 °C. $^1$H NMR (500 MHz, $C_6D_6$, $\delta$): 8.57, 8.19, 7.65 (br), 7.29, 7.00, 3.79, 2.02, 1.60, 1.48, 1.41, 1.38, −4.55. UV-vis (toluene at 25 °C) $\lambda_{max}$ ($\varepsilon$ [mM$^{-1}$ cm$^{-1}$]): 306 (21 080), 327 (sh) (19 800), 430 (5900), 448 (sh) (5400), 545 (6440). Anal. Calcd for $C_{50}H_{66}Fe_2N_4S_2$: C, 66.81; H, 7.40; N, 6.23. Found: C, 66.90; H, 7.24; N, 6.18.

**Preparation of Se$_8$.** Red $Se_8$ was prepared according to a literature procedure.[32] To a stirred, heated solution of concentrated sulfuric acid (100 ml, 150 °C) was slowly added grey selenium (1.00 g, 1.27 mol). The reaction mixture was refluxed until it turned to dark green (*ca.* 12 h). Upon cooling, the reaction mixture was filtered and the filtrate was slowly added to ice (250 g). After the ice had completely melted, the red precipitate was collected through vacuum filtration and was washed using deionized water until the filtrate was neutral. Red $Se_8$ was then washed with ethanol and then with diethyl ether (950 mg, 95%).

**Cautious:** When handling and heating concentrated $H_2SO_4$, it is imperative to exercise utmost caution given its strong corrosive properties and potential hazards.

**[(L1)Fe(μ-Se)]$_2$ (2).** To a stirred solution of $Se_8$ (119 mg, 0.19 mmol) in toluene (5 mL) at ambient temperature under $N_2$ atmosphere was added 100 mg (0.19 mmol) of LFe$^I$(cod) in toluene (15 mL). The resulting slurry was stirred for 48 h at ambient temperature. The reaction mixture was filtered twice through $Al_2O_3$. The filtrate was dried *in vacuo*, and the residue was extracted with *n*-pentane and filtered through Celite. Volatiles were removed under reduced pressure to afford a dark teal solid (57 mg, 60%). Crystals suitable for X-ray diffraction were grown from a concentrated *n*-pentane solution of the complex at −20 °C. $^1$H NMR (500 MHz, $C_6D_6$, $\delta$): 8.75, 8.36, 7.64 (br), 7.28, 6.98, 3.41, 2.28, 2.21, 1.72, 1.61, 1.46, 1.28, 1.16, −6.05. UV-vis (toluene at 25 °C) $\lambda_{max}$ ($\varepsilon$ [mM$^{-1}$ cm$^{-1}$]): 319 (20 560), 434 (2880), 613 (3000). Anal. Calcd for $C_{50}H_{66}Fe_2N_4Se_2$: C, 60.13; H, 6.59; N, 5.72. Found: C, 60.31; H, 6.44; N, 5.83.

### Electrochemistry

Cyclic voltammetry was conducted using a CH-Instruments electrochemical analyzer (model 620E), employing a 3 mm glassy carbon working electrode, a silver wire pseudo-reference electrode, and a platinum coiled wire counter electrode. All measurements were performed using THF solutions, containing 1 mM analyte and 0.1 M N(Bu)$_4$PF$_6$ as the supporting electrolyte. The potentials were referenced to a ferrocene/ferrocenium redox couple.

### Crystallography

Data were collected using a Rigaku Rapid II curved image plate diffractometer with Cu-Kα radiation ($\lambda$ = 1.54178 Å). Single crystals were mounted on a Mitegen micromesh mount using a trace of Fomblin oil and cooled *in situ* to at 100 K. Data were processed using HKL3000 and the data were corrected for absorption and scaled using Scalepack.[33] The space groups were assigned using XPREP within the SHELXTL suite of programs,[34,35] were solved by direct methods using ShelXS and refined by full matrix least squares against $F^2$ with all reflections using Shelxl2018 using the graphical interface ShelXle.[36] H atoms attached to carbon atoms were positioned geometrically and constrained to ride on their parent atoms, with carbon hydrogen bond distances of 0.95 Å for alkene and

Published on 01 ervna 2023. Downloaded on 01.02.2026 21:36:21.

aromatic C–H, 1.00 and 0.98 Å for aliphatic C–H and $CH_3$, respectively. $U_{iso}$(H) values were set to a multiple of $U_{eq}$(C) with 1.5 for $CH_3$ and 1.2 for C–H groups respectively.

### Kinetic measurements

Pseudo-first-order reaction conditions were employed for all kinetic studies, using 20-fold and greater excesses of $^{32}S_8$ or $^{34}S_8$. Reactions were monitored by UV-Vis spectroscopy. Due to the low solubility of $S_8$, low concentrations of (**L1**)Fe(cod) were used in kinetic experiments. Typically, 3 mL of a toluene solution containing the (**L1**)Fe(cod) complex (0.3 μmol) in a sealable cuvette under $N_2$ was placed in a temperature-controlled cryostat. Upon temperature equilibration, a toluene solution of $^{32}S_8$ or $^{34}S_8$ was added rapidly *via* syringe. Spectra were taken at 30 s to 45 min intervals. The reaction was followed by monitoring the increase in one of the ligand-to-metal charge transfer (LMCT) absorption bands used to indicate the formation of **1**. Nonlinear least-squares fitting of the absorbance at 545 nm using a first-order model yielded the pseudo-first-order rate constants, $k_{obs}$. The transition state parameters were determined over a temperature range of −40 to −70 °C and *via* an Eyring plot, which shows a linear relationship. S/Se atom transfer reactions were performed by mixing (**L1**)Fe(cod) complex (9.5 μmol) with an excess of $S_8$ or $Se_8$ and $PPh_3$ in $C_6D_6$ at 40 °C and monitored by $^1$H NMR spectroscopy. The formation of S=$PPh_3$ and Se=$PPh_3$ were quantified with respect to hexamethylbenzene (internal standard). Each parameter reported represents the average value of duplicate or triplicate determinations.

## Results and discussion

### Syntheses

**1** was synthesized by the reaction of $S_8$ with (**L1**)Fe(cod) at room temperature (Scheme 2). Immediately a color change of the solution from green to dark purple was observed. However, when treating $Se_8$ with (**L1**)Fe(cod) to yield **2**, the reaction occurred at a much slower rate with a gradual color change to teal over the course of several hours. Note that reactions run at lower temperature did not produce significantly improved yields. At room temperature, the $^1$H NMR spectra of compounds **1** and **2** display characteristics of paramagnetism, manifesting as broadening and up-field shifted peaks (−4.5 and −6.0 ppm for **1** and **2**, respectively), despite most of the resonances lying within the diamagnetic region. The β-methyl protons are responsible for the paramagnetic chemical shifts, which can also be observed in other [2Fe–2S] model compounds containing β-diketiminate ligands (−0.4 ppm for **3** and −8.1 ppm for **4**).[26,27] The magnetic properties of synthetic [2Fe–2E] model compounds are primarily determined by strong antiferromagnetic coupling between the two high-spin $S$ = 5/2 $Fe^{3+}$ ions.[19–21,23,24] The presence of an antiferromagnetic coupled dimer was evident by measuring the magnetic moment of **1** and **2** in $C_6D_6$ which were found to be by Evan's method 1.2 and 1.3$\mu_B$, respectively. The values agree with those of other reported [LFe(μ-E)]$_2$ complexes.

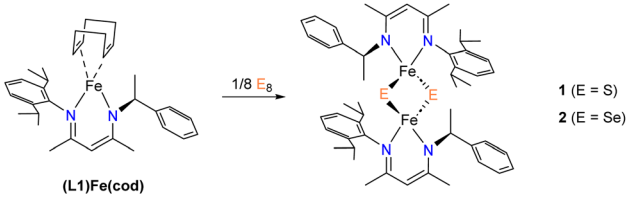


Scheme 2 Synthesis of **1** and **2**.

### Crystal structures of 1 and 2

Single crystals suitable for X-ray structure determination were obtained for complex **1** and **2**. The ORTEP diagrams of **1** and **2** are given in Fig. 1 and selected bond lengths and angles are summarized in Table 1 and Table S1.† The solid-state structures confirm complexes **1** and **2** as binuclear iron complexes, where each iron center is coordinated by two N atoms from a β-diketiminate ligands and two bridged S atoms (**1**) or Se atoms (**2**) (Fig. 1). The molecular geometry of the metal ion in **1** ($\tau_4$ = 0.847) and **2** ($\tau_4$ = 0.932) is best described as distorted tetrahedral. For **1**, the average Fe–N distances of 1.989(7) Å agrees with those of other β-diketiminate supported complexes of [2Fe–2S] clusters bearing high-spin Fe(III) centers.[26,27] However, the average bond distances of Fe–S (2.377(3) Å) and inter-atomic distance of Fe···Fe (3.360(2) Å) are much longer than any of the reported values for other synthetic [2Fe–2S] model compounds. On the other hand, the average bond distance of Fe–Se (2.317(7) Å) and inter-atomic distance of Fe···Fe (2.750(3) Å) in **2** are only slightly longer than those in [(Pipiso)Fe(μ-Se)]$_2$ (Pipiso = [(DipN)$_2$C(*cis*-2,6-$Me_2NC_5H_8$)]$^-$, (Dip = 2,6-$C_6H_3{}^iPr_2$). Interestingly, the Fe···Fe distance in [(Pipiso)Fe(μ-E)]$_2$ (E = O, S, Se) reflects the size of bridging chalcogenide ligands, but the opposite trend was found for **1** and **2**.[23] Therefore, by comparing the crystal structures of **1** and **2** the unusual Fe···Fe distance found in **1** can be attributed to the steric effect of methyl groups pointing toward the aryl ring.

The Fe···Fe distance for most [2Fe–2S] model complexes are typically in a small range of 2.69–2.82 Å, which are smaller

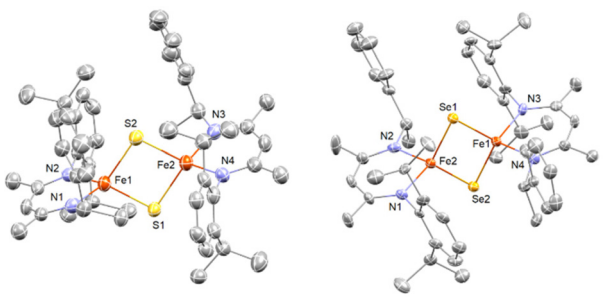


Fig. 1 X-ray crystal structures of **1** (left) and **2** (right). Thermal ellipsoids shown at 50% probability, hydrogen atoms and solvate molecules (toluene, pentane) omitted for clarity. Color key: orange = Fe, blue = N, gray = C, yellow = S, gold = Se.


This journal is © the Partner Organisations 2023

Published on 01 ervna 2023. Downloaded on 01.02.2026 21:36:21.

Table 1 Selected averaged bond distances (Å) and angles (°) for **1–6** [a]

| | **1** (E = S) | **3** [26] | **4** [27] | **5** [25] | **2** (E = Se) | **6** [29] |
|---|---|---|---|---|---|---|
| Fe–N | 1.989(7) | 1.973(5) | 2.004(1) | 2.028(2) | 1.983(5) | 1.996(2) |
| Fe–E | 2.377(3) | 2.204(2) | 2.194(1) | 2.210(1) | 2.317(1) | 2.318(1) |
| ∠N–Fe–N | 94.6(3) | 97.7(2) | 93.23(6) | 91.64(8) | 96.1(3) | 92.6(1) |
| ∠E–Fe–E | 90.07(9) | 105.49(7) | 104.72(2) | 100.82(3) | 107.23(8) | 107.46(2) |
| ∠Fe–E–Fe | 89.83(9) | 74.51(6) | 75.28(2) | 79.18(2) | 72.77(7) | 72.55(2) |
| Fe⋯Fe | 3.360(2) | 2.669(1) | 2.679(1) | 2.816(1) | 2.750(3) | 2.743(1) |
| N–Fe–Fe–N[b] | 11.17 | 2.44 | 8.43 | 1.93 | 1.92 | 5.66 |
| $\tau_4$ | 0.816 | 0.910 | 0.891 | 0.895 | 0.932 | 0.913 |

[a] Numbers in parentheses are standard uncertainties in the last significant figures. Atoms are labeled as indicated in Fig. 1. [b] Torsion angle is defined by a dihedral angle between two N–Fe–N planes.

than protein [2Fe–2S] clusters.[19–24,26,27,37,38] It is known that a short Fe⋯Fe distance is one of the contributions for strong antiferromagnetic coupling between two Fe(III) centers.[39] However, diamagnetism of complex **1** suggests antiferromagnetic coupling occurring in solution although the Fe⋯Fe distance is rather long in solid state. In comparison of [2Fe$^{III}$–2S] with the super-reduced cluster, [2Fe$^{II}$–2S], the difference of their Fe⋯Fe distances is <0.1 Å.[21,24] Furthermore, long Fe⋯Fe distances (3.2 to 3.4 Å) are often observed in thiolate-bridged complexes [2Fe$^{II}$-2SR],[40–42] which may imply that complex **1** is a [2Fe$^{II}$-2SH] cluster compound and the hydrogen atoms were not resolved by X-ray crystallography. However, this possibility can be ruled out since no characteristic S–H stretching vibrations were observed in **1**.

In addition, although some monosulfido-bridged Fe(II) complexes are diamagnetic,[43,44] most [2Fe$^{II}$-2SR] complexes are paramagnetic with large magnetic moments.[40–42] Hence, **1** is most likely a [2Fe$^{III}$–2S] model compounds with an unusual long Fe–Fe distance resulting from the steric repulsion between the two β-diketiminate ligands. The steric profiles were also suggested by the $\tau_4$ values among all [2Fe–2S] model complexes supported by β-diketiminate ligands (Table 1). In addition, as the steric bulkiness increases, the torsion angle between the two chelated faces (N–Fe–N) increases (Table 1 and Fig. S1†).

### Electrochemical and UV–vis studies of complex 3 and 4

Cyclic voltammetry of complex **1** (Fig. 2) suggests there are two quasi-reversible events occurring, while there is only one quasi-reversible event observed for complex **2** (Fig. S2†). These events indicate the electron transfer is a diffusion controlled process which was confirmed by the linear relationship in the plot of peak current *vs.* square root of the scan rate (Fig. 2 inset). The first quasi-reversible event of **1** appears at −1.68 V and the second is at −2.13 V. However, the peak height of the first event is twice as large as the second event. This suggests the first event may involve two times the number of electrons with respect to the second event. To understand the number of electrons transferred based on the voltammograms, titration of complex **1** with a chemical reductant, bis-pentamethylcyclopentadienylcobalt(II) ($CoCp^*_2$) was monitored using UV-vis spectroscopy. Since the second quasi-reversible event of **1** is

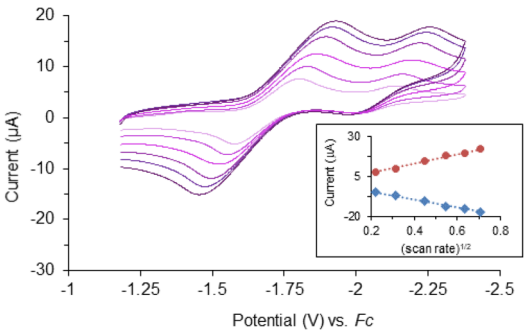


Fig. 2 Overlaid cyclic voltammograms of **1** (1 mM) in THF with 0.1 M $N(Bu)_4PF_6$. Scan rates = 50, 100, 200, 300, 400, 500 mV $s^{-1}$ referenced to a ferrocene/ferrocenium redox couple (Fc). Inset: plot of cathodic peak current (●, $R^2$ = 0.9953) and anodic peak current (◆, $R^2$ = 0.9962) *versus* square root of scan rate.

at −2.13 V, we can use this chemical reductant, whose redox potential is −1.94 V, to investigate only the first electron transfer process at −1.61 V.

Complex **1** shows three major LMCT bands (300, 431, and 545 nm) which are consistent with those observed in other model compounds and Rieske-type proteins with the oxidation state of both iron ions being 3+.[23,29,45,46] Complex **2**, on the other hand, exhibits two charge-transfer bands that are bathochromically shifted compared to **1** (Fig. S3†). The red-shift of the LMCT bands is consistent with the trend of ligand field transition energy of the bridging atoms. These features diminished upon titration with reductant, $CoCp^*_2$ (Fig. 3). Further addition of the chemical reductant past two equivalents did not show any additional change. Therefore, the 2 : 1 ($CoCp^*_2$: **1**) molar ratio suggests the first quasi-reversible event of **1** involves two electrons and implies the second event is a one-electron process. The single quasi-reversible event of complex **2** is at −1.91 V and could represent the transfer of one or two electrons. Similarly, titration of **2** with $CoCp^*_2$ was monitored by using UV-vis spectroscopy at $\lambda_{max}$ = 614 nm, which diminished and did not show any change after addition of 1 equiv. of $CoCp^*_2$ (Fig. S4†). Therefore, this 1 : 1 ($CoCp^*_2$: **2**) molar ratio suggests that the single quasi-reversible event of **2** involves one electron. Attempts to reduce **1** were encouraged by the quasi-reversible redox events and relatively stable in

Published on 01 ervna 2023. Downloaded on 01.02.2026 21:36:21.

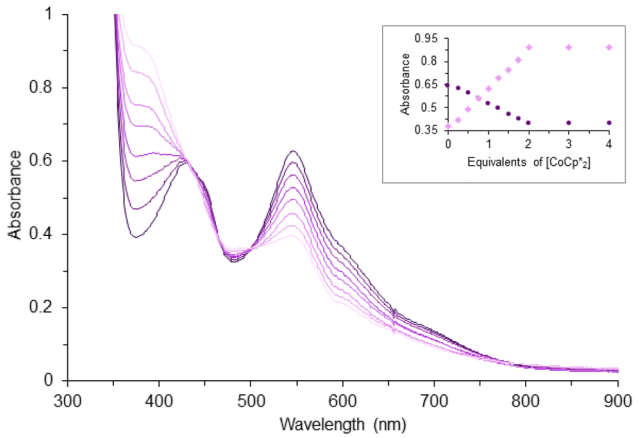


Fig. 3 Reduction of 0.1 mM **1** in THF by addition of $CoCp^*_2$ in increments of 0.25 equiv. as monitored by UV-vis spectroscopy (path length, 1.0 cm). Inset: corresponding changes of the absorbance at 389 (♦) and 545 (●) nm.

THF solution upon reduction. However, the reactions led to intractable products through many trials under different conditions (*e.g.* variety of reductants, solvents, and temperatures). Although several reduced species supported by other bidentate nitrogen-donor ligands were successfully synthesized and reported,[21,24,26,27] the futile attempts for isolating the reduction products of **1** could be due to the unusually long Fe···Fe distance.

### Kinetic studies of the formation of 1

Since the synthesis of [2Fe–2S] model compounds are not always straightforward, with attempts often yielding homoleptic complexes, $L_2Fe$ (L = bidentate ligands), an alternative procedure was discovered by the oxidation of elemental sulfur with mono- or di-nuclear Fe(I) precursors.[23,24,26] Therefore, to gain insights into the formation of **1**, we carried out kinetic studies for the activation of elemental sulfur with the low-valent Fe complex, (**L1**)Fe(cod). When the observed rate constants $k_{obs}$ are plotted as a function of the concentration of $S_8$, a linear dependence that, within error, passes through the origin is observed (Fig. S5 and S6†). These data indicate a bimolecular reaction between (**L1**)Fe(cod) and $S_8$. When comparing the rates for reactions conducted under the same conditions with $^{34}S_8$, the kinetic isotopic effect (KIE) of $k^{32}S_8/k^{34}S_8$ = 1.02. The normal KIE value suggests that the rate-determining step is likely the cleavage of the S–S bond, but we cannot completely rule out the possibility of experimental errors based on this value. More insights into the formation mechanism of **1** from (**L1**)Fe(cod) and $^{32}S_8$ was gained from temperature-dependence kinetic experiments. An Eyring analysis over a temperature range of −40 to −70 °C gave the activation parameters $\Delta^{\ddagger}H$ = 17.0 ± 0.6 kJ mol$^{-1}$ and $\Delta^{\ddagger}S$ = −155 ± 8 J mol$^{-1}$ K$^{-1}$ which correspond to an associated $\Delta^{\ddagger}G_{298\ K}$ = 63.2 ± 0.8 kJ mol$^{-1}$ (Fig. S7†). The positive enthalpy of activation presumably implies cleavage of the S–S bond in the transition state. The large negative entropy of activation suggests the reaction proceeds *via* an associative mechanism and could be due to the formation of a highly ordered transition state where a partially broken S–S bond of the $S_8$ molecule chelates the Fe center.

### Sulfur atom transfer studies

Albeit still under debate, sulfur atom transfer reactions in enzymes with [2Fe–2S] clusters may play an important role in metabolic reactions *e.g.* biotin synthase transforms dethiobiotin to biotin. Considering the long Fe–S bond length, **1** could be a suitable candidate for an S-atom transfer reaction. When treating **1** with $PPh_3$ at 40 °C, the formation of S═$PPh_3$ was observed by $^1$H NMR spectroscopy. This result has encouraged us to further study the potential catalytic S-atom transfer reaction. However, due to the limited solubility of $S_8$, it was not possible to obtain consistent kinetic data when using excess (10-fold) amounts of $S_8$. Thus, the only viable approach to determine whether the iron complex catalyzes the S-atom transfer reaction is to obtain the overall yields of S═$PPh_3$ from reaction of **1** with triphenyl phosphine. Direct reaction of $S_8$ with $PPh_3$ was expected to be a much slower process. Since Fe(I) species are considered to be generated after transferring an S atom from **1**, we tested if catalytic atom transfer is possible by mixing an Fe(I) precursor, (**L1**)Fe(cod), with excess $S_8$ and $PPh_3$. The mixture was maintained at 40 °C for one hour and the formation of S═$PPh_3$ was confirmed and quantified (yield = 70%) by $^{31}$P and $^1$H NMR spectroscopy.[47] Conversely, in the absence of (**L1**)Fe(cod), only 11% conversion was observed. Scheme S1† presented the proposed reaction mechanism, whereby mixing (**L1**)Fe(cod) with $S_8$ resulted in the immediate formation of **1**, which subsequently reacted with $PPh_3$ to generate S═$PPh_3$. The residual two-coordinate Fe(I) species could form species **A** through binding with an excess amount of triphenylphosphine ligand(s). Note that the two-coordinate Fe(I) species or **A** may act as an active catalyst, or alternatively, the regeneration of (**L1**)Fe(cod) could occur through ligand substitution of free cyclooctadiene and triphenylphosphine ligand (s). The Se atom transfer reaction, under the same conditions, was slower, regardless of the presence (12%) or absence (5%) of (**L1**)Fe(cod).

## Conclusions

This study reports two [2Fe–2E] model compounds, [(**L1**)Fe(μ-S)]$_2$ (**1**) and [(**L1**)Fe(μ-Se)]$_2$ (**2**), supported by a chiral diketiminate ligand. The presence of steric hindrance in **1** is believed to be the cause of its remarkably elongated Fe···Fe distance, which is thought to have played a role in the failure to synthesize reduced [2Fe–2S] compounds. **1** is capable of transferring three electrons whereas a single electron redox event is observed in **2**. For the formation of **1**, kinetic analysis suggests that the cleavage of the S–S bond is the rate-determining step and the reaction proceeds *via* an associative mechanism. The highly efficient S-atom transfer reaction could be attributed to the unusually long Fe–S bond length in **1**, and these results imply that S-atom transfer reactions may occur in biological

 This journal is © the Partner Organisations 2023

relevant [2Fe–2S] clusters. The ongoing research is to gain further insight into the reaction mechanism of E-atom transfer reactions with the goal of facilitating the efficient synthesis of chiral E-containing compounds by utilizing these [2Fe–2E] model complexes as catalysts.

## Author contributions

Erwin A. Weerawardhana: writing original draft, synthesis and characterization of compounds. Matthias Zeller: crystallography. Wei-Tsung Lee: experimental design, supervision, data validation, manuscript review, and editing. All authors have given approval to the final version of the manuscript.

## Conflicts of interest

There are no conflicts to declare.

## Acknowledgements

This work was supported by start-up funds (Loyola University Chicago). The X-ray diffractometers were funded by National Science Foundation through the Major Research Instrumentation Program under grants no. CHE 1625543 (Purdue University). We thank Dr Daniel J. McElheny (University of Illinois at Chicago) for acquiring $^{31}$P-NMR spectra.

## References

1 H. Beinert, R. H. Holm and E. Münck, Iron-sulfur clusters: nature's modular, multipurpose structures, *Science*, 1997, **277**, 653–659.
2 J. C. Crack, J. Green, A. J. Thomson and N. E. L. Brun, Iron–Sulfur Clusters as Biological Sensors: The Chemistry of Reactions with Molecular Oxygen and Nitric Oxide, *Acc. Chem. Res.*, 2014, **47**, 3196–3205.
3 E. L. Mettert and P. J. Kiley, Fe-S proteins that regulate gene expression, *Biochim. Biophys. Acta*, 2015, **1853**, 1284–1293.
4 J. A. Santos, N. Alonso-García, S. Macedo-Ribeiro and P. J. Pereira, The unique regulation of iron-sulfur cluster biogenesis in a Gram-positive bacterium, *Proc. Natl. Acad. Sci. U. S. A.*, 2014, **111**, E2251–E2260.
5 W. R. Hagen, in *Adv. Inorg. Chem*, ed. R. Cammack, Academic Press, 1992, vol. 38, pp. 165–222.
6 A. P. Bali, D. Lennox-Hvenekilde, N. Myling-Petersen, J. Buerger, B. Salomonsen, L. S. Gronenberg, M. O. A. Sommer and H. J. Genee, Improved biotin, thiamine, and lipoic acid biosynthesis by engineering the global regulator IscR, *Metab. Eng.*, 2020, **60**, 97–109.
7 F. Berkovitch, Y. Nicolet, J. T. Wan, J. T. Jarrett and C. L. Drennan, Crystal structure of biotin synthase, an S-adenosylmethionine-dependent radical enzyme, *Science*, 2004, **303**, 76–79.
8 B. T. Bui, D. Florentin, F. Fournier, O. Ploux, A. Méjean and A. Marquet, Biotin synthase mechanism: on the origin of sulphur, *FEBS Lett.*, 1998, **440**, 226–230.
9 K. J. Gibson, D. A. Pelletier and I. M. Turner Sr., Transfer of sulfur to biotin from biotin synthase (BioB protein), *Biochem. Biophys. Res. Commun.*, 1999, **254**, 632–635.
10 J. T. Jarrett, Biotin synthase: enzyme or reactant?, *Chem. Biol.*, 2005, **12**, 409–410.
11 C. Sirithanakorn and J. E. Cronan, Biotin, a universal and essential cofactor: synthesis, ligation and regulation, *FEMS Microbiol. Rev.*, 2021, **45**, 1–18.
12 S. B. Yu, G. C. Papaefthymiou and R. H. Holm, Comprehensive iron-selenium-thiolate cluster chemistry, *Inorg. Chem.*, 1991, **30**, 3476–3485.
13 J. G. Reynolds and R. H. Holm, Core chalcogenide atom substitution reactions of $[Fe_2X_2(SR)_4]^{2-}$ and $[Fe_4X_4(SR)_4]^{2-,3-}$ clusters (X = sulfur, selenium), *Inorg. Chem.*, 1981, **20**, 1873–1878.
14 J. M. Moulis and J. Meyer, Characterization of the selenium-substituted 2[4Fe-4Se] ferredoxin from Clostridium pasteurianum, *Biochemistry*, 1982, **21**, 4762–4771.
15 T. M. Buscagan, J. T. Kaiser and D. C. Rees, Selenocyanate derived Se-incorporation into the nitrogenase Fe protein cluster, *eLife*, 2022, **11**, e79311.
16 J. T. Henthorn, R. J. Arias, S. Koroidov, T. Kroll, D. Sokaras, U. Bergmann, D. C. Rees and S. DeBeer, Localized Electronic Structure of Nitrogenase FeMoco Revealed by Selenium K-Edge High Resolution X-ray Absorption Spectroscopy, *J. Am. Chem. Soc.*, 2019, **141**, 13676–13688.
17 F. Fabrizi de Biani and P. Zanello, The competition between chemistry and biology in assembling iron-sulfur derivatives. Molecular structures and electrochemistry. Part IV. {[Fe3S4](SγCys)3} proteins, *Inorg. Chim. Acta*, 2017, **455**, 319–328.
18 P. Zanello, The competition between chemistry and biology in assembling iron–sulfur derivatives. Molecular structures and electrochemistry. Part V. {[Fe4S4](SCysγ)4} proteins, *Coord. Chem. Rev.*, 2017, **335**, 172–227.
19 A. Albers, T. Bayer, S. Demeshko, S. Dechert and F. Meyer, A Functional Model for the Rieske Center: Full Characterization of a Biomimetic N-Ligated [2Fe-2S] Cluster in Different Protonation States, *Chem. – Eur. J.*, 2013, **19**, 10101–10106.
20 J. Ballmann, X. Sun, S. Dechert, E. Bill and F. Meyer, Relatively stable N-ligated $[2Fe2S]^{2+}$ clusters with dipyrromethane capping ligands, *J. Inorg. Biochem.*, 2007, **101**, 305–312.
21 A. Albers, S. Demeshko, K. Pröpper, S. Dechert, E. Bill and F. Meyer, A Super-Reduced Diferrous [2Fe–2S] Cluster, *J. Am. Chem. Soc.*, 2013, **135**, 1704–1707.
22 A. Albers, S. Demeshko, S. Dechert, E. Bill, E. Bothe and F. Meyer, The Complete Characterization of a Reduced Biomimetic [2Fe-2S] Cluster, *Angew. Chem., Int. Ed.*, 2011, **50**, 9191–9194.
23 L. Fohlmeister, K. R. Vignesh, F. Winter, B. Moubaraki, G. Rajaraman, R. Pöttgen, K. S. Murray and C. Jones,

Published on 01 ervna 2023. Downloaded on 01.02.2026 21:36:21.

Published on 01 ervna 2023. Downloaded on 01.02.2026 21:36:21.

Neutral diiron(III) complexes with $Fe_2(\mu\text{-}E)_2$ (E = O, S, Se) core structures: reactivity of an iron(I) dimer towards chalcogens, *Dalton Trans.*, 2015, **44**, 1700–1708.

24 Q. Liang, J. C. DeMuth, A. Radović, N. J. Wolford, M. L. Neidig and D. Song, [2Fe–2S] Cluster Supported by Redox-Active o-Phenylenediamide Ligands and Its Application toward Dinitrogen Reduction, *Inorg. Chem.*, 2021, **60**, 13811–13820.

25 R. G. Castillo, A. W. Hahn, B. E. Van Kuiken, J. T. Henthorn, J. McGale and S. DeBeer, Probing Physical Oxidation State by Resonant X-ray Emission Spectroscopy: Applications to Iron Model Complexes and Nitrogenase, *Angew. Chem., Int. Ed.*, 2021, **60**, 10112–10121.

26 M. E. Reesbeck, M. M. Rodriguez, W. W. Brennessel, B. Q. Mercado, D. Vinyard and P. L. Holland, Oxidized and reduced [2Fe–2S] clusters from an iron(I) synthon, *J. Biol. Inorg. Chem.*, 2015, **20**, 875–883.

27 S. Yao, F. Meier, N. Lindenmaier, R. Rudolph, B. Blom, M. Adelhardt, J. Sutter, S. Mebs, M. Haumann, K. Meyer, M. Kaupp and M. Driess, Biomimetic [2Fe-2S] Clusters with Extensively Delocalized Mixed-Valence Iron Centers, *Angew. Chem., Int. Ed.*, 2015, **54**, 12506–12510.

28 J. T. Henthorn, G. E. Cutsail, T. Weyhermüller and S. DeBeer, Stabilization of intermediate spin states in mixed-valent diiron dichalcogenide complexes, *Nat. Chem.*, 2022, **14**, 328–333.

29 C. Panda, P. W. Menezes, C. Walter, S. Yao, M. E. Miehlich, V. Gutkin, K. Meyer and M. Driess, From a Molecular 2Fe-2Se Precursor to a Highly Efficient Iron Diselenide Electrocatalyst for Overall Water Splitting, *Angew. Chem., Int. Ed.*, 2017, **56**, 10506–10510.

30 E. A. Weerawardhana, A. Pena, M. Zeller and W.-T. Lee, Synthesis and characterization of iron and cobalt complexes with an asymmetric N-alkyl,N′-aryl-β-diketiminate ligand, *Inorg. Chim. Acta*, 2017, **460**, 29–34.

31 E. M. Schubert, Utilizing the Evans Method with a Superconducting NMR Spectrometer in the Undergraduate Laboratory, *J. Chem. Educ.*, 1992, **69**, 62.

32 J. Ebels, S. Spirk and R. Pietschnig, Presented in part at the Proceedings of the 10th International Electronic Conference on Synthetic Organic Chemistry, Basel, Switzerland, 1–30 November 2006, 2006.

33 Z. Otwinowski and W. Minor, in *Methods Enzymol*, Academic Press, 1997, vol. 276, pp. 307–326.

34 *SHELXTL, 6.14; Bruker Advanced X-ray Solutions*, Bruker AXS Inc., Madison, Wisconsin, USA, 2000–2003.

35 G. Sheldrick, A short history of SHELX, *Acta Crystallogr., Sect. A: Found. Crystallogr.*, 2008, **64**, 112–122.

36 G. Sheldrick, Crystal structure refinement with SHELXL, *Acta Crystallogr., Sect. C: Cryst. Struct. Commun.*, 2015, **71**, 3–8.

37 J. Ballmann, S. Dechert, S. Demeshko and F. Meyer, Tuning Electronic Properties of Biomimetic [2Fe-2S] Clusters by Ligand Variations, *Eur. J. Inorg. Chem.*, 2009, **2009**, 3219–3225.

38 J. Ballmann, X. Sun, S. Dechert, B. Schneider and F. Meyer, A convenient ligand exchange pathway to [2Fe–2S] ferredoxin analogues, *Dalton Trans.*, 2009, 4908–4917, DOI: **10.1039/B901242G**.

39 J. J. Mayerle, R. B. Frankel, R. H. Holm, J. A. Ibers, W. D. Phillips and J. F. Weiher, Synthetic analogs of the active sites of iron-sulfur proteins. Structure and properties of bis(o-xylyldithiolato-$\mu_2$-sulfidoferrate (3)), an analog of the 2Fe-2S proteins, *Proc. Natl. Acad. Sci. U. S. A.*, 1973, **70**, 2429–2433.

40 D. Sellmann, J. Utz and F. W. Heinemann, Transition-Metal Complexes with Sulfur Ligands. 132. Electron-Rich Fe and Ru Complexes with $[MN_2S_3]$ Cores Containing the New Pentadentate Ligand '$N_2H_2S_3'^{2-}$ (=2,2′-Bis(2-mercaptophenylamino)diethyl Sulfide(2−)), *Inorg. Chem.*, 1999, **38**, 459–466.

41 L. Wang, M. Gennari, F. G. Cantú Reinhard, S. K. Padamati, C. Philouze, D. Flot, S. Demeshko, W. R. Browne, F. Meyer, S. P. de Visser and C. Duboc, $O_2$ Activation by Non-Heme Thiolate-Based Dinuclear Fe Complexes, *Inorg. Chem.*, 2020, **59**, 3249–3259.

42 D. K. Mills, Y. M. Hsiao, P. J. Farmer, E. V. Atnip, J. H. Reibenspies and M. Y. Darensbourg, Applications of the $N_2S_2$ ligand, N,N'-bis(mercaptoethyl)-1,5-diazacyclooctane (BME-DACO), toward the formation of bi- and heterometallics: $[(BME\text{-}DACO)Fe]_2$ and $[(BME\text{-}DACO)NiFeCl_2]_2$, *J. Am. Chem. Soc.*, 1991, **113**, 1421–1423.

43 C.-Y. Lu and W.-F. Liaw, Formation Pathway of Roussin's Red Ester (RRE) via the Reaction of a {Fe(NO)2}10 Dinitrosyliron Complex (DNIC) and Thiol: Facile Synthetic Route for Synthesizing Cysteine-Containing DNIC, *Inorg. Chem.*, 2013, **52**, 13918–13926.

44 S. E. Creutz and J. C. Peters, Diiron Bridged-Thiolate Complexes That Bind N2 at the FeIIFeII, FeIIFeI, and FeIFeI Redox States, *J. Am. Chem. Soc.*, 2015, **137**, 7310–7313.

45 D. Coucouvanis, A. Salifoglou, M. G. Kanatzidis, A. Simopoulos and V. Papaefthymiou, Dimeric complexes containing the disulfidodiiron(2+) cores coordinated by non-sulfur containing terminal ligands. The crystal and molecular structures of the tetraethylammonium salts of the $[Fe_2S_2(o,o'\text{-}C_{12}H_8O_2)_2]^{2-}$ and $[Fe_2S_2(C_4H_4N)_4]^{2-}$ anions, *J. Am. Chem. Soc.*, 1984, **106**, 6081–6082.

46 M. E. Konkle, S. K. Muellner, A. L. Schwander, M. M. Dicus, R. Pokhrel, R. D. Britt, A. B. Taylor and L. M. Hunsicker-Wang, Effects of pH on the Rieske Protein from Thermus thermophilus: A Spectroscopic and Structural Analysis, *Biochemistry*, 2009, **48**, 9848–9857.

47 T. A. Albright, W. J. Freeman and E. E. Schweizer, Nuclear magnetic resonance studies. IV. Carbon and phosphorus nuclear magnetic resonance of phosphine oxides and related compounds, *J. Org. Chem.*, 1975, **40**, 3437–3441.

 This journal is © the Partner Organisations 2023